Fuel 334 (2023) 126816

Contents lists available at ScienceDirect

Fuel

journal homepage: www.elsevier.com/locate/fuel

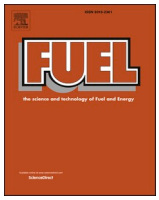

Full Length Article

Synthetic oxygen carrier C28 compared to natural ores for chemical looping combustion with solid fuels in 80 kW_{th} pilot plant experiments

Fleiß Benjamin [a,*], Priscak Juraj [b], Fuchs Josef [a], Müller Stefan [a], Hofbauer Hermann [a]

[a] Institute of Chemical, Environmental and Bioscience Engineering, TU Wien, Austria
[b] BEST – Bioenergy and Sustainable Technologies GmbH, Austria

A B S T R A C T

Chemical Looping Combustion (CLC) is a highly efficient CO_2 separation technology with no direct contact between combustion air and fuel. A metal oxide is used as oxygen carrier (OC) in a dual fluidized bed to generate clean CO_2. The use of solid fuels, especially biomass, is the focus of current research, because of the possibility of "negative" CO_2-emissions. The OC is a key component, because it must meet special requirements for solid fuels, which are different to gaseous fuels. Most frequently naturals ores or synthetic materials are used as OC. Synthetic OC are characterised by higher reactivity at the expense of higher costs. For this reason, so far not so many experiments have been conducted on a larger scale with synthetic OC on solid CLC. This work deals with the synthetic perovskite C28 and investigating the suitability as oxygen carrier in an 80 kW_{th} pilot plant for chemical looping combustion with biogenic fuels. The experiments show a significantly increased combustion efficiency of 99.6 % compared to natural ores and a major influence of the solid circulation rate on general performance, whereby carbon capture rates up to 98.3 % were reached. Furthermore, the role of the fuel reactor's counter-current flow column and its impact on better gas conversion was investigated. C28 suffered no deactivation or degradation over the experimental time, but first traces of ash layer formation, phase shifting and attrition of fines could be detected. The focus of further research should lie on long-term stability and reactivity for their high impact on the economic scale up of C28.

1. Introduction

Chemical looping combustion (CLC) is one of the most efficient carbon capture technology utilizing the oxygen capacity of certain metal oxides, called oxygen carrier (OC), to combust fuel to clean CO_2. There is no direct mixing of combustion air and fuel and therefore the exhaust gas is not contaminated by nitrogen [1]. Using biomass as fuel, CLC as a bioenergy with carbon capture and storage (BECCS) technology enables "negative" CO_2 emissions, what will be required to achieve the climate targets [2,3]. Facing addition challenges with solid fuels, there are two major levers to improve the CLC process, on the one hand the reactor design and on the other hand finding suitable OC. In the case of OC, either cheap natural ores respectively residual materials or highly specialized synthetic OC are used. [4] The high cost of synthetic OC is then reflected in higher conversion rates and therefore cleaner CO_2, which reduces the gas treatment costs. A disadvantage is the contamination by fuel ash and the resulting deactivation of the expensive OC during the process. Since few synthetic OC have been tested in larger plants due to their high costs, this work deals with one of the first utilization of the synthetic oxygen carrier C28 in an 80 kW_{th} pilot plant in comparison to natural ores. The used synthetic perovskite type oxygen carrier C28 showed already promising results for gas CLC applications [5,6]. During the experiments, important process parameters and the possibility of optimization of the reactor design were investigated during operation. The experimental results were validated by a simulation model and in addition, in-depth analyses of the bed material were carried out.

1.1. Theory

CLC is an unmixed combustion technology, where an oxygen carrier provides pure oxygen for the combustion of fuel. The OC is transported through two different reactors with two different reaction zones, see Fig. 1. In the first reaction step, located in the air reactor (AR), the oxidation (Eq. (1)) of the OC takes place, where the OC binds oxygen during a reaction with air. In the fuel reactor (FR) and during the second reaction zone (Eq. (2)), the transfer of oxygen to the fuel (C_nH_m) happens. [7] The OC releases oxygen and due to the absence of nitrogen, the product gas consists of CO_2 and H_2O. Thereby the OC is reduced and oxidation is necessary for further usage of the material. [8] The circulation of OC between the reactors transfers the oxygen necessary for combustion and the heat required to maintain the heat balance in the system.

$$Me_xO_{y-1} + 1/2\ O_2 \rightarrow Me_xO_y \quad (1)$$

* Corresponding author at: Getreidemarkt 9/166 1060 Wien-A.
E-mail address: benjamin.fleiss@tuwien.ac.at (F. Benjamin).

https://doi.org/10.1016/j.fuel.2022.126816
Received 19 September 2022; Received in revised form 7 November 2022; Accepted 15 November 2022
Available online 26 November 2022

Symbols and Abbreviations

AR	Air reactor
BECCS	Bioenergy with Carbon Capture & Storage
C28	Synthetic perovskite oxygen carrier
CLC	Chemical looping combustion
CLOU	Chemical looping with oxygen uncoupling
C_nH_m	Fuel
DFB	Dual fluidized bed
FR	Fuel reactor
ILS	Inner loop seal
LLS	Lower loop seal
Me_yO_x	Metal oxide
OC	Oxygen carrier, oxygen carriers
OP	Operation point
SCR	Solid circulation rate
TGA	Thermogravimetric analysis
ULS	Upper loop seal
UV	Ultraviolet
XRD	X-ray diffraction analysis
g [m/s^2]	Gravitational acceleration
m [g]	Mass of OC
m_o [g]	Oxidized mass of OC
$m_{FR,spez}$ [kg/MW]	Fuel power specific Fuel reactor filling with OC
m_r [g]	Reduced mass of OC
$\dot{n}_{C,FR,exhaust}$ [mol/s]	mol flow of carbon FR exhaust
$\dot{n}_{CO2,FR,exhaust}$ [mol/s]	mol flow of carbon dioxide FR exhaust
$\dot{n}_{C,FR,feed}$ [mol/s]	mol flow of carbon FR fuel feed
$\dot{n}_{O_2,fuel,dem}$ [mol/s]	mol flow of oxygen for combustion FR fuel feed
$\dot{n}_{O_2,exhaust,dem}$ [mol/s]	mol flow of oxygen for combustion FR exhaust
$P_{fuel,FR}$ [kW$_{th}$]	Fuel power input of the fuel reactor
P_{oil} [kW$_{th}$]	Oil power input to the air reactor
R_{calc} [–]	Empirical factor for calculating the solid circulation
$R_{O\ CLOU}$ [kg/kg]	Oxygen transport of uncoupling oxygen
S/C [–]	Steam to carbon ratio
SCR [kg/h]	Solid circulation rate between air and fuel reactor
SCR_{calc} [kg/h]	Calculated solid circulation rate based on pressure
SCR_G [kg/m^{2}s]	Mean global solid circulation rate
SCR_{spec} [kg/kWh$_{th}$]	Specific solid circulation rate based on power
S_n [%]	Selectivity of certain gas specie
S_{CO2} [%]	Selectivity of gas specie CO_2
tol_{xi} [–]	Tolerance of the mean value
$V_{AR,sec}$ [nm^3/h]	Secondary volume flow air reactor
$V_{AR,tert}$ [nm^3/h]	Tertiary volume flow air reactor
$V_{Add,air}$ [nm^3/h]	Addition volume flow air reactor
X_C [%]	Carbon conversion
x_i [–]	calculated value
$\overline{x_i}$ [–]	Mean value
X_{S_ULS} [%]	Oxidation state upper loop seal
Y_{CO2} [%]	Yield of CO_2
Y_n [%]	Yield of certain gas specie
ΔH [m]	Height between pressure measurements
Δp [mbar]	Pressure gradient in FR
η_{CC} [%]	Carbon capture rate
η_{comb} [%]	Combustion efficiency
ϑAR_{exh} [°C]	Temperature of air reactor exhaust gas
ϑFR_{exh} [°C]	Temperature of fuel reactor exhaust gas
ϑFR_{low} [°C]	Temperature of lower fuel reactor
λ [–]	Air to fuel ratio
φ [kg/kg]	Oxygen of OC to fuel ration
Ω_{OD} [%]	Oxygen demand for full combustion

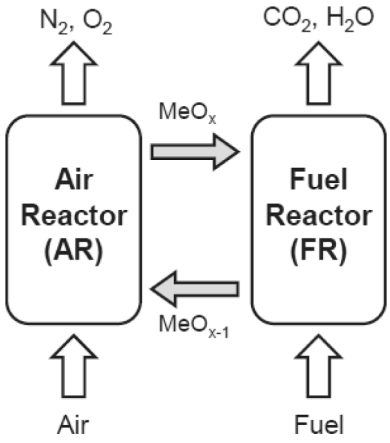

Fig. 1. Scheme of the CLC process with AR and FR.

$$(2n+m)\ Me_yO_x + C_nH_m \rightarrow (2n+m)\ Me_yO_{x-1} + n\ CO_2 + m/2\ H_2O \quad (2)$$

The cornerstone for the CLC technology is the oxygen carrier and the materials must fulfil a number of different criteria in order to be suitable for operation. They must have sufficient oxygen transport capacity (R_O), with high reactivity both for reduction and oxidation reactions, and be maintained over a large number of redox cycles. The oxygen transport capacity is calculated with the fully oxidized mass of oxygen carrier m_o and fully reduced mass m_r. [1]

$$R_O = \frac{m_o - m_r}{m_o}\ [kg/kg] \quad (3)$$

OC also need to have favorable thermodynamics with regard to fuel conversion to CO_2 and H_2O. Good fluidization properties and no agglomeration in the reactors are fundamental for stable operation. A key point is the resistance to attrition in order to reduce losses of elutriated fines and replacement costs of OC. Economical oxygen carriers, such as ilmenite, iron or manganese ores, and iron containing wastes have mainly been proposed for usage with solid fuels in CLC. A disadvantage is that the mentioned materials show no permanent chemical looping with oxygen uncoupling (CLOU) effect which is beneficial for the CLC processes. The instability of a formed oxide can trigger the partial release of the oxygen under certain conditions of temperature and oxygen partial pressure. Through that, a direct homogeneous combustion reaction is possible and this increases the fuel conversion rates in the FR considerable. A number of synthetic Cu- and Mn-based OC are developed for CLOU combustion of solid fuels [9]. High CO_2 efficiencies and high combustion rates are obtained with these types of OC. The disadvantage of synthetic OC is the high price and therefore deactivation through ash dilution and attrition is critical for economic operation.

2. Material and methods

2.1. 80 kWth CLC pilot plant

Several CLC pilot plants of various sizes have already been commissioned for research purposes. The next commercial scale up step is still pending, but the dual fluidized bed (DFB) system has shown the highest potential for reactor models of larger scale. Among the plants that can be found in literature are a 100 kW$_{th}$ reactors located at Chalmers University of Technology, a 3 MW$_{th}$ plant erected by Alstom and a 1 MW$_{th}$ pilot plant at Darmstadt University of Technology. Other

concepts focus on smaller facilities, like an 1.5 kW_{th} reactor operated by the Spanish National Research Council. [10] An 80 kW_{th} pilot plant at TU Wien has also been proposed as DFB system by Pröll and Hofbauer [11] for solid fuel CLC and Schmid et al. [12] for fluidized bed steam gasification, see Fig. 2 and Fig. 3. The plant consists of two fluidized beds, the air reactor (AR) and the fuel reactor (FR), which are connected at the top and bottom via steam fluidized loop seals. These loop seals function as gas lock between the reactors to ensure the CO_2 purity as well as high carbon capture rates. The AR is designed as fast fluidized bed and works as riser for the OC to ensure circulation of the bed material between the reactors. Air can be introduced at three different levels. This air staging enables a control over the solid circulation of bed material, transported to the FR. The entrained particles from the AR are separated by a gravity separator and transported to the FR via the upper loop seal (ULS) [13,14]. The FR is divided into two different zones. The lower part is designed as bubbling fluidized bed with high solids inventory to ensure proper solids residence time and char gasification. The upper part of the FR working as a counter current column has internals placed along its height, reducing the free cross section of the reactor. These constrictions intensify the gas-solid contact by increasing the solid hold up. The free cross section area of the internals can be adapted by an adjustable rod, brown colored in Fig. 5. Due to lower gas velocities in the FR only minimal solids entrainment occur and a counter-current flow of particles and gas is obtained in the upper part. The FR is operated with steam, which also function as gasification agent for solid fuels. The particles that are elutriated from the upper part of the FR are recirculated again back through a gravity separator and the internal loop seal (ILS) to the bottom part of the FR. The solids loop is closed by the lower loop seal (LLS), where the particles are transported again to the AR. For

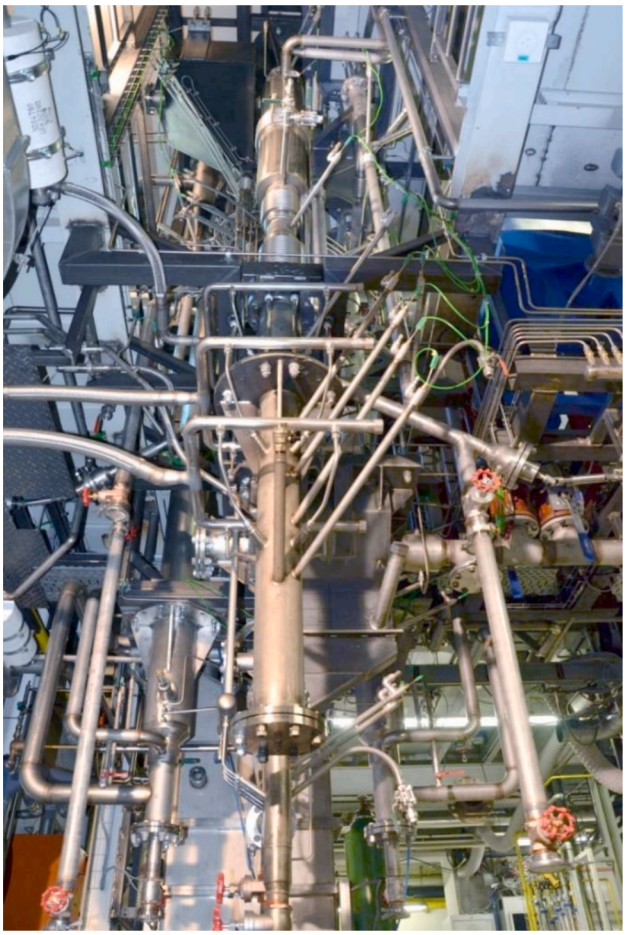

Fig. 2. 80 kW_{th} pilot plant at TU Wien without insulation.

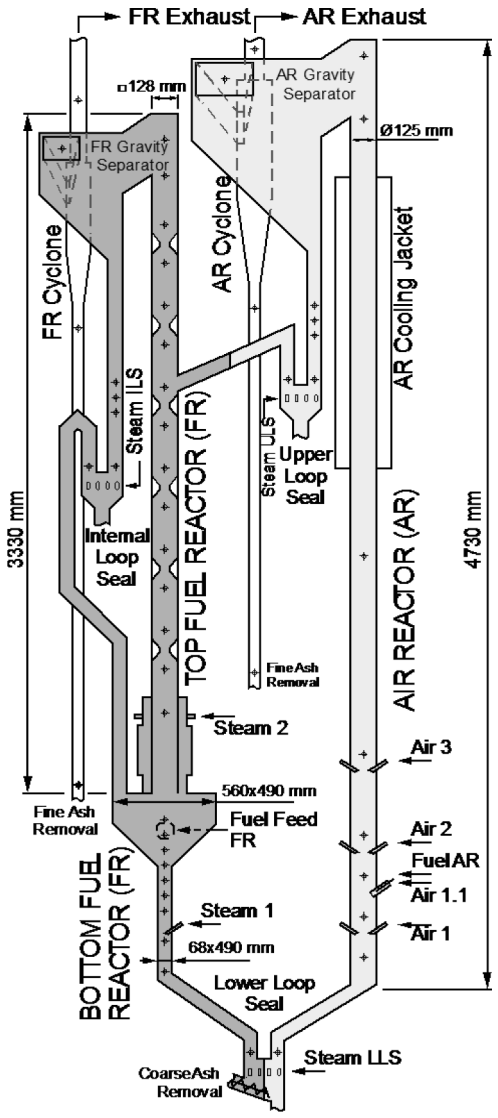

Fig. 3. Scheme of the 80 kW_{th} pilot plant at TU Wien, divided into FR on the left and AR on the right side.

secondary solid separation of fine entrainment, both the AR and the FR are equipped with high efficiency cyclones. The fuel is fed into the lower part of the FR by on-bed feeding via a screw conveyer. Auxiliary fuel in form of fuel oil can be introduced to the AR to compensate for high heat losses caused by the large specific surface area of the pilot plant. The exhaust gas stream of the two reactors were continuously monitored with respect to O_2, CO_2, and CO (AR) as well as CO_2, CO, CH_4, H_2 and O_2 (FR) by Rosemount NGA 2000 gas analyzers (UV/IF, paramagnetic and heat conductivity). In addition, gas chromatography is used to determine N_2 and higher hydrocarbons in the FR exhaust gas.

The pilot plant is in operation since 2015 [15] and the work so far included investigations with different fuels and different bed materials [16–19]. The first solid CLC experimental campaign was conducted and published 2018 [20].

2.2. Oxygen carrier

The synthetic OC used in this work, called C28, was originally developed by Chalmers University of Technology and VITO [21]. Production of C28 was scaled up using industrially available raw materials and infrastructure during the EU funded project SUCCESS for gaseous CLC [22,23]. The leftover material was used for solid CLC, for which the

OC was also originally developed. The batch – internally referred as Lana – used for this work was produced by industrially relevant raw materials and production methods. The raw materials were dispersed in demineralized water. The so produced slurry was milled using ZrO_2 beads. After a polymer binder was added, the slurry was spray-dried to particles. The fraction between 150 and 300 μm was calcinated in a stationary kiln and the remaining fraction was re-dispersed. [24] The resulting perovskite structure of $CaMn_{0,775}Mg_{0,1}Ti_{0,125}O_{3-\delta}$ is a dark gray sand like powder. The material shows a high oxygen transport capacity and also the CLOU effect, releasing gaseous oxygen under reducing conditions. In Fig. 4 a comparison to ilmenite, an intensively researched OC is shown from literature [25,26]. The kinetics of C28 have been investigated by Abad et al. in thermal gravimetric analysis (TGA) [27]. The elemental analysis is given in Table 1.

The fresh OC material used in this work was extensively investigated before utilization in the pilot plant. The particle size distribution was measured by means of a laser diffraction technique with a Malvern Mastersizer 2000. The mean particle diameter and the bulk density are given in Table 2. The formed crystalline phases were analyzed by X-ray powder diffraction (XRD) using a Philips X'Pert diffractometer with PANalytical X'Pert Pro software, see Table 2.

In addition, the OC was assessed and characterized by a method established by Fleiβ et al. [28]. Fig. 6 shows important properties in a spider chart in comparison to ilmenite. C28 does not only reach a higher total area in the chart, but shows also superior properties, especially on the left side of the diagram, which indicates the oxygen carrier specific properties of the materials. The synthetic OC shows higher oxygen transport, carbon conversion and CO_2 yields than all tested natural ores so far. However, the lower bulk density and density of the material can have negative effects, since less of the OC overall fits into the plant and the heat transport from AR to FR is more limited. The pilot plant was filled with 55 kg of C28, in comparison to experiments with ilmenite, where 80 kg of OC were used.

2.3. Fuels

As fuel two different types of pellets were used. Softwood pellets of class EN-plus A1 according to ISO 17225–2 with a diameter of 6 mm and a length of 3 – 40 mm, are characterized by a low ash content and sulphur/chlorine content. This fuel was mainly used for heat up and as reference fuel to previous experiments.

Bark pellets were the second fuel for the experiments. Table 3 shows the results of the fuel analysis. For the bark pellets a similar combustion behavior as with soft wood pellets can be expected but with containing higher amount of ash. For this reason, the bark pellets are well suited to investigate degradation of the OC in contact with ash. The ash composition and ash melting temperature, see Table 4, make the fuel ideal for studying the formation of ash surfaces on the OC without affecting the operation through agglomeration.

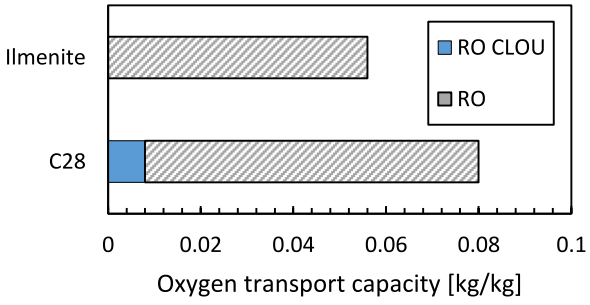

Fig. 4. Oxygen transport capacity R_O of C28 with the ratio of CLOU oxygen in comparison to ilmenite.

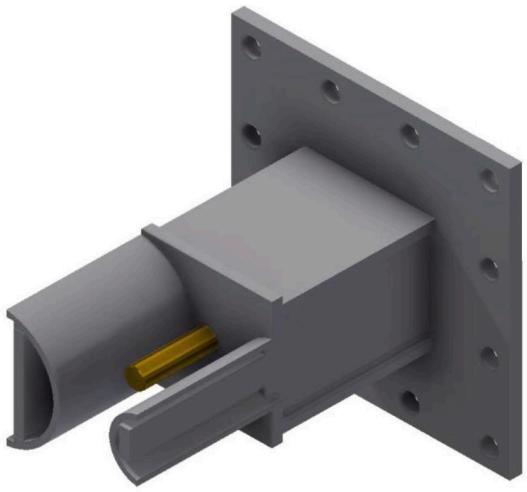

Fig. 5. Constriction with adjustable tube to further decrease the cross section of the counter current column.

Table 1
Elemental analysis of C28.

C28 (LANA)	Element	[%]	Element	[%]
	Al	0.03	Mn	31.70
	Ca	27.10	S	0.13
	Fe	0.54	Si	0.13
	Mg	2.33	Ti	4.51

Table 2
Physical and chemical properties of the fresh C28.

Parameter	Value
XRD main phases	$Ca((Mn_{0.9}Ti_{0.1})O_{2.961}$, MgO, $CaMn_2O_4$
Mean particle size [μm]	139
Bulk density [kg/m^3]	1780

2.4. Validation of experimental results by simulation

The mass and energy balance modelling and data evaluation of the experiments were performed using the simulation software IPSEpro from Simtech Simulation Technology. It is a stationary, equation oriented software for the simulation of power and chemical plants and can be used for quick, preliminary process evaluation, detail engineering and design, monitoring and optimization of existing plants as well as for statistical validation of measurement data. Standardized components, so-called units, are already established based on mathematical equations and variables. These units and equations are formulated in a way that mass and energy balances are strictly fulfilled for each unit. Based on the units the model or flow sheet, of the complete process is built, see Fig. 7. This process model is used together with the property data to build a single system of (non-linear) equations which is numerically solved using the Newton-Raphson method. Detailed information about the structure of model-units and the Newton-Raphson method can be found in literature, Marx et al. [29]. Within the context of this work, the model was used to validate the stationary operational points and the important measurements of each experiment to calculate the full mass and energy balance.

The model of the 80 kW_{th} CLC pilot plant for solid fuels has been built using the Advanced Energy Technology library (AET library) which has been especially designed for chemical looping based processes. To describe the thermodynamic state of streams and substances involved, the following property data is used and addition information are found at Bolhar-Nordenkampf et al. [30]:

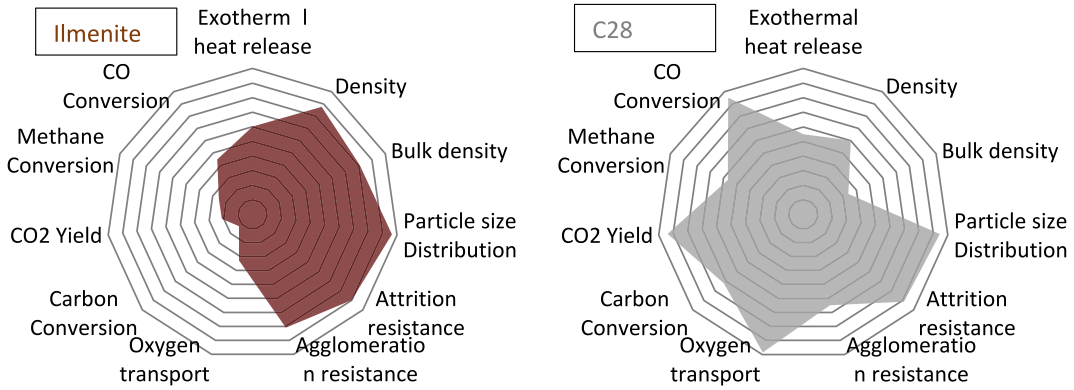

Fig. 6. Spider chart of the important properties of C28 in comparison to the natural ore ilmenite.

Table 3
Fuel analysis of softwood and bark.

		Softwood	Bark
Water content	wt%	7.2	16.1
Ash	wt%(wf)	0.2	20.7
Carbon	wt%(wf)	50.7	45.03
Hydrogen	wt%(wf)	5.9	3.4
Oxygen	wt%(wf)	43.0	30.1
Nitrogen	wt%(wf)	0.2	0.7
Sulphur	wt%(wf)	0.0	0.06
Chlorine	wt%(wf)	0.0	<0.01
Volatiles	wt%(waf)	85.4	69.9
LHV (dry)	kJ/kg(wf)	18,900	16,400

Table 4
Ash melting behavior and elemental composition of bark ash.

		Bark	
Softening point	°C	1160	
Hemisphere temperature	°C	1230	
Flow temperature	°C	1390	
Element	w%	Element	w%
Mo	0.2	Cr	0.1
Nb	0.2	V	0.1
Zr	0.2	Ti	0.5
Sr	0.2	Ca	11.9
Pb	0.1	K	7.2
As	–	Cl	0.2
Zn	0.1	S	0.2
Cu	0.1	P	0.3
Ni	0.1	Si	23.4
Co	0.1	Al	6.1
Fe	2.7	Mg	1.2
Mn	0.6	Na	1.6
O	42.6		

- Pure water/steam according to IAPWS-IF97 (Wagner and Kruse, 1998) [31].
- Mixtures of ideal gases according to Burcat and Gardiner (2000) [32].
- Organic substances composed of C, H, N, O, S and Cl according to Barin and Platzki (1995) [33].
- Inorganic solids (active and non-active) according to Barin and Platzki (1995) [33].

This also includes formulation of several redox-systems based on Cu, Fe, Mn, Ni, CaS and Co including inert support materials like Al_2O_3, $MgAl_2O_4$, SiO_2, TiO_2 and ZrO_2. For C28, as a simplification, the redox-system of Mn_2O_3/MnO was used. Models of gas-solid reactors for chemical looping processes also include chemical equilibrium formulations of important reactions like the water-gas-shift reaction, the interaction between CO and metal oxides and the oxidation reaction in the AR.

$$\sum_i \left(\frac{x_i - \bar{x}_i}{tol_{x_i}}\right) \rightarrow min \tag{4}$$

The simulation tool can also be used for the verification of measurement data based on closing mass and energy balances of the modelled 80 kW_{th} pilot plant. The required data is the mean values of measurements like pressures, temperatures, flow rates, gas concentrations and oxidation state of the OC for certain time intervals during steady state operation. The set of measured data is used together with the process model to create an overdetermined system of equations, i.e., it has more equations than variables. Additionally, a tolerance is assigned to each measurement value reflecting its quality and deviations during the observed time interval. This overdetermined system of equations can be solved using the method of Lagrange multipliers, see Eq. (4), resulting in a least squares problem for the deviation between measured values and balanced solution:

The balanced solution of the measurement data reflects the most probable operation condition of the investigated operating point within the model structure fulfilling mass and energy balances. Based on the calculated balances, to evaluate and assess the performance of the OC and the operating, important parameters must be taken into consideration. The carbon capture rate η_{CC}, defined in Eq. (5), describes how much of the carbon fed into the fuel reactor is found in the gas phase of the fuel reactor exhaust gas. This also represents the loss of carbon, mainly through combustion in the air reactor.

$$\eta_{CC} = \frac{\dot{n}_{C,FR,exhaust}}{\dot{n}_{C,FR,feed}} \bullet 100\ [\%] \tag{5}$$

The CO_2 yield γ_{CO2} describes how much of the carbon introduced into the fuel reactor is contained in the fuel reactor exhaust gas as CO_2. It is a measure of incomplete conversion of fuel carbon to CO_2 and given by Eq. (6) and it includes the loss of carbon to the AR as well as elutriated char.

$$\gamma_{CO_2} = \frac{\dot{n}_{CO_2,FR,exhaust}}{\dot{n}_{C,FR,feed}} \bullet 100\ [\%] \tag{6}$$

The CO_2 selectivity S_{CO2} is a measure whether the combustion of the carbon $\dot{n}_{C,FR,exhaust}$ in the exhaust gas to CO_2 is complete. The rest of Eqs. (7) to 100 % represents the amount of unburnt carbon in the gas like components of CO, CH_4, higher hydrocarbons and tars.

$$S_{CO_2} = \frac{\dot{n}_{CO_2,FR,exhaust}}{\dot{n}_{C,FR,exhaust}} \bullet 100\ [\%] \tag{7}$$

The combustion efficiency η_{Comb} describes how much of the fuel is actual converted to CO_2 and H_2O. It combines the unconverted gases with the lost fuel to the AR reactor and gives an overall assessment of the

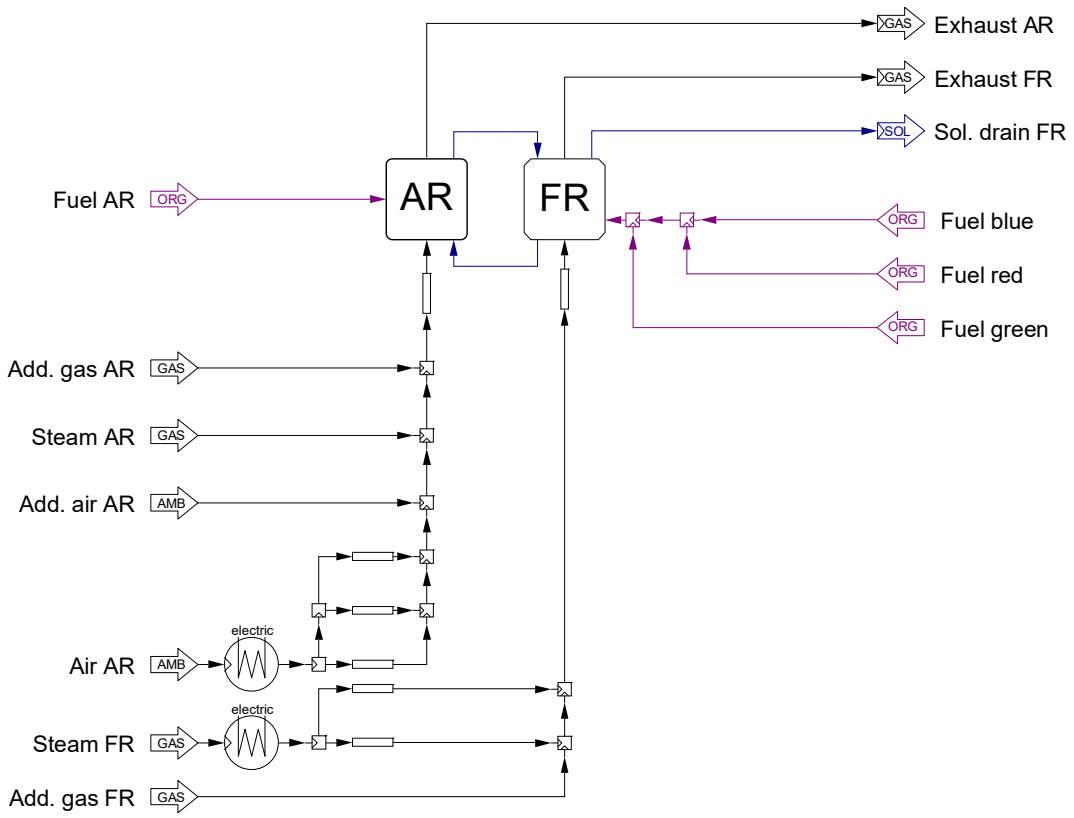

Fig. 7. Basic simulation flow chart of the of the 80 kW_{th} pilot plant based on units in IPSEpro.

CLC operation, shown in Eq. (8). It is based on ratio of the demanded oxygen for complete stoichiometric combustion of the exhaust gas $\dot{n}_{O_2,fuel,dem}$ and of the fuel $\dot{n}_{O_2,fuel,dem}$.

$$\eta_{Comb} = \left(1 - \frac{\dot{n}_{O_2,exhaust,dem}}{\dot{n}_{O_2,fuel,dem}}\right) \bullet 100\ [\%] \tag{8}$$

The total oxygen demand Ω_{OD} describes the amount of oxygen necessary for complete oxidation of the FR exhaust gas compared to the amount of oxygen necessary for full oxidation of the fuel feed, see Eq. (9).

$$\Omega_{OD} = \frac{\dot{n}_{O_2,exhaust,dem}}{\dot{n}_{O_2,fuel,dem}} \bullet 100\ [\%] \tag{9}$$

$$X_S = \frac{m - m_r}{m_O - m_r} \bullet 100\ [\%] \tag{10}$$

Furthermore, it is important to validate the oxidation state of the solid samples in hot operation. The oxygen loading of an OC was evaluated over several cycles in the following experiments. The oxidation level of the OC can be determined by Eq. (10) as the solid conversion of OC X_S. [34] The variable m denotes the instantaneous mass of the OC, while m_r and m_o indicate the masses at full reduction and full oxidation. Kolbitsch et al. (2009) shows a method determining X_S of a solid sample with a simple procedure in a furnace. [35]

$$SCR_{calc} = \frac{\Delta p \bullet \dot{V}_{AR,sum}}{\Delta H \bullet g} \bullet R_{calc}\ [\mathrm{kg/h}] \tag{11}$$

Two ways of calculating the solid circulation rate *SCR* were applied. The first value results from the simulation based on the transported oxygen, heat transport and measured X_S from solid sampling. SCR_{calc} is based on Fuchs et al. [36], see Eq. (11), which specify a correlation between pressure drop Δp in the upper AR and solid circulation rate applied to DFB systems. R_{calc} is an empirical factor based on the pressure gradient in the upper AR and ranges from 0.2 to 0.4.

3. Results and discussion

3.1. Start-up and general operation

The start-up procedure of the pilot plant was divided into two different phases: During the first phase, the fluidization of the AR and FR (air for both reactors) was preheated up to 500 °C using electrical heating. When the plant temperature reached 400 °C, fuel in form of light fuel oil (AR) and wood pellets (FR) was fed into the plant. At 850–900° C, the air fed to the FR was gradually replaced by steam. Additionally, the fluidization agent of the loop seals was changed from air to steam until full steam fluidization and also CLC operation was reached. Once steam was added to the FR fluidization, the OC started to transport oxygen from AR to FR and oxidation of fuel in the FR happened. The temperature difference between FR bottom and FR top increases caused by endothermal gasification reactions in the bottom region. Gas composition in the FR changes towards high CO2 concentration and some remaining unconverted gas species (CO, H2, CH4). During CLC operation, no significant problems caused by e.g., agglomeration of bed material. The solid circulation of the OC was controlled by air staging in the AR. A limitation took place on the one hand by the size of the loop seals (ULS, LLS) and on the other hand by flooding of the counter current column of the FR. Flooding means the filling of the counter current column and the subsequent uncontrolled discharge of the OC from the reactor. This is caused by a combination of high gas volume and high OC quantity in the upper part of the FR, which is dependent on solid circulation rate and amount of fuel. Furthermore, it was ensured that 1100 °C was not exceeded, since this limit is specified by the material of the reactor. Fig. 8 shows the composition of the FR exhaust gas and temperatures of AR and FR over the first experimental day. At around 17:00 the fuel was changed to bark pellets. This triggered a slight decrease in temperature. The CO_2 concentration was high at approximately 93 %, whereby the other unburnt components CH_4, CO, H_2 were always below 1.5 %. The concentrations of CO and H_2 were

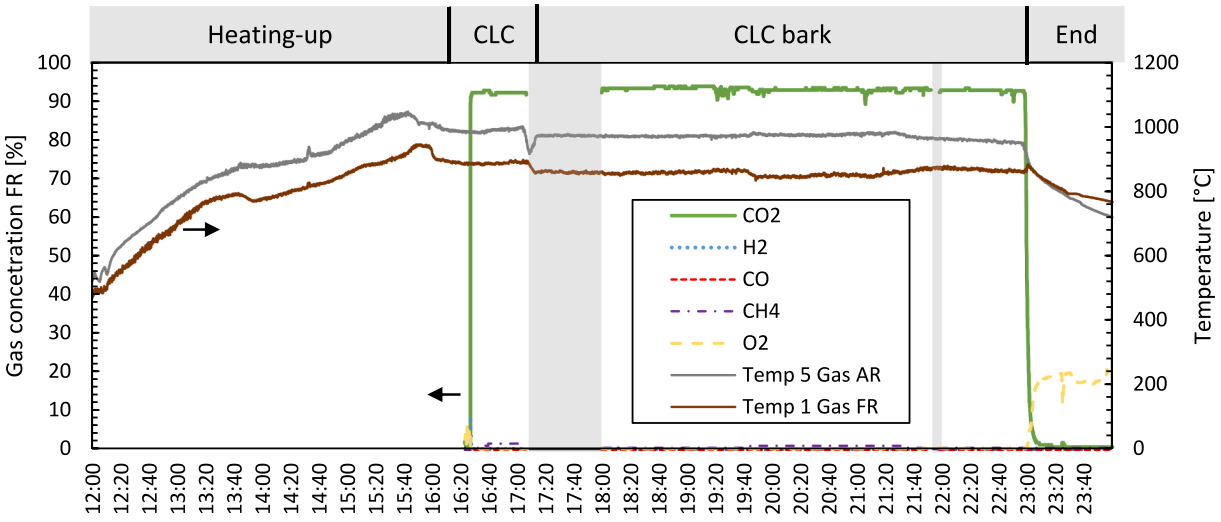

Fig. 8. Gas concentrations of FR and temperatures of AR and FR over the duration of the experimental day.

even below the detection limits of the gas measurements. The majority of the rest gas was nitrogen, which was used for flushing of pressure measurements and the fuel bunkers. The grey areas are no disruption of operation, but adapting and cleaning of the gas measurement. During steady state operation, only minimal deviation of the measured values occurred. In total, over 16 h of successful and stable CLC operation with the OC C28 was achieved.

3.2. Influence of solid circulation

To investigate the impact of solid circulation rate *SCR* of C28 on the OC performance three different operating points were conducted, see Table 5. For comparison, both the *SCR* based on the simulation and SCR_{calc} based on the pressure drop measurements are given. By shifting the air from tertiary to primary air, the *SCR* could be increased and vice versa. Lana_1.1 showed medium, Lana_1.2 the lowest and Lana_1.3 the highest *SCR*, which is consistent with the air staging. Air staging is a well-functioning tool to control the *SCR*, but has also limitations. For example, it should be noted that for Lana_1.3, the fuel rate had to be slightly reduced to prevent the column from flooding. The difference between the oxidation states ΔX_S of the OC of the upper loop seal ULS and lower loop seal increased with lower *SCR, see also* Fig. 9. That means the OC had to transport more oxygen per kg OC.

The analysis of the solid samples of the upper loop seal $X_{S\ ULS}$ in a furnace also showed that the C28 was not fully oxidized in the AR during the experiments. This possibly led to no available CLOU oxygen in FR to fully convert the fuel. This was also confirmed by the fact that no oxygen was measured in the FR during the CLC operation and it is possible also the result of insufficient residence time of the OC in the AR. Regarding accuracy, the method of determining X_S, was developed for gas CLC and won't show exact values because of ash and char in the solid sample [35]. For better performance of the OC, it could be beneficial to increase the OC to fuel ratio and the air to fuel ratio. This are parameters to better compare the different operating points. Lana_1.3 has the highest values because of higher *SCR* and lower amount of fuel. The air to fuel ratio of Lana_1.1 is slightly lower because of the different total volume flow of air. The total oxygen demand indicates the quality of the combustion and how much additional oxygen would be necessary for full combustion. Lana_1.3 would have needed an addition of below 1 % of the stoichiometric oxygen for full combustion of the bark pellets.

The effect of the *SCR* on operation was very clear. With high *SCR* the conversion to CO_2 and of other gases was promoted, see Fig. 10. The concentration of CO, CH_4, higher hydro-carbons and tars was reduced with higher *SCR*. The carbon capture rate seems in contrast to be affected negatively by higher *SCR*, showed via Lana_1.3. In principle, a higher *SCR* means a lower residence time of OC particles in the FR. Unburnt fuel and char are carried along with the OC and therefore reduce the carbon capture rate of the process. The two opposing effects have to be balanced during operating and could be for example reconciled by reactor design decisions. This can mean the adapting of the bubbling bed, height of FR counter current column or installing a carbon stripper. The tar concentration of Lana_1.3 was not measured, but estimated by a correlation between gravimetric tars and the methane concentration [37].

3.3. Comparison with natural ores

In order to compare the synthetic OC with natural ores, the results of former experimental campaigns in the 80 kW_{th} pilot plant were used. This involved seven experimental days with over 50 h of solid CLC operation with three different OC and five fuels. Table 6 shows the stable operating points that were obtained during the experimental campaigns with the most important process conditions and performance parameters. During all experiments stable CLC operation was reached and the pilot plant proved to be flexible in regard to OC and fuel. High carbon captures rates over 95 % were continuously achieved. The combustion efficiency was higher than 68 % with each OC, but changed fundamentally based on the operating state and ramped up to 90 % with the right settings. Temperatures between 900 and 1050 °C were investigated. Depending on the OC, operating conditions and fuel, auxiliary

Table 5
Three operating points of the Lana experiments with different SCR, controlled via air staging.

OP	$V_{AR,prim}$	$V_{AR,sec}$	$V_{AR,tert}$	$V_{Add,air}$	$V_{AR,sum}$	$m_{FR,spez}$	ΔX_S	SCR	SCR_{calc}	SCR_G
[text]	[Nm^3/h]	[Nm^3/h]	[Nm^3/h]	[Nm^3/h]	[Nm^3/h]	[kg/MW]	[%]	[kg/h]	[kg/h]	[kg/m^2s]
Lana_1.2_low	11.0	15.6	27.7	4.0	49.3	725	26.7	**901**	**1010**	**20.5**
Lana_1.1_mid	14.1	16.0	21.6	4.0	46.1	659	15.0	**1102**	**1080**	**25.1**
Lana_1.3_high	20.0	16.7	17.7	4.0	50.9	882	10.1	**1285**	**1309**	**29.2**

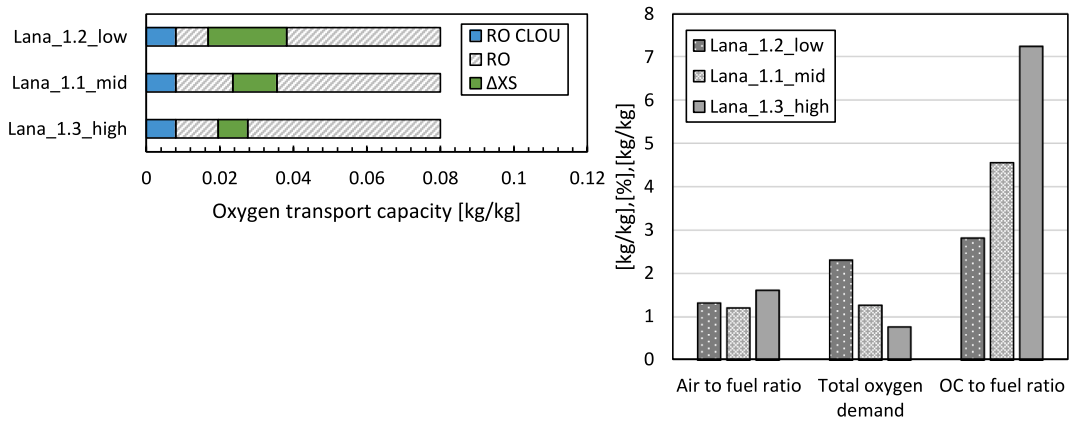

Fig. 9. Oxygen transport capacity R_O and solid conversion X_S to the left and addition parameters of operation on the right side, comparing different solid circulation rate.

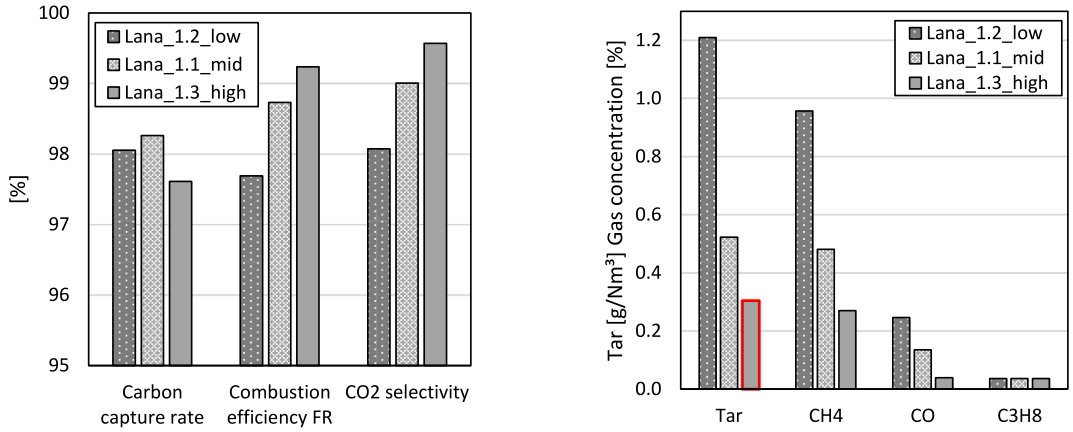

Fig. 10. Performance parameters on the left and unburnt components on the right side for the three operating points comparing impact of solid circulation rate.

fuel in form of oil had to be used to maintain temperatures. Also, heat losses over the reactor could be compensated by adding oil (P_{oil}) to the AR. At the same time, however, a partial reduction of the OC takes place in the AR. As a result, more air must be used in the AR in order to oxidize the OC sufficiently, and therefore CLC operation is slightly hindered. In successful CLC operation, however, the heat transport should compensate for heat losses and provide enough heat transport to the FR, to achieve autothermal operation. In this regard, stable operation was almost impossible to achieve with the manganese ore (MnOre_1). Due to insufficient heat transport caused by the low density, the only way of reaching stable operating conditions was achieved by adding oil in the AR. Another important parameter is the *SCR*, whereby a general decrease could be observed over time with braunite as OC. In the course of the experimental campaign, braunite was filled into the reactor twice to replace the loss of bed material. The stress on the material during CLC operation, where the material undergoes several reduction and oxidation reactions in a short time, is increased. Ilmenite proved to be more resistant to attrition than the manganese containing OC. During the test runs with ilmenite (Ilmenite_2.1), the material was undergoing an activation that led to higher conversion and capture rates in autothermal operation. With ilmenite the highest *SCR* could be reached due to its high density. From the used natural ores, ilmenite also showed the most promising results [28]. However, the highest conversion of gas in the FR was reached with the synthetic OC C28 with a CO_2 selectivity of 99.6 %. The high reactive perovskite reached nearly full combustion and good carbon capture rates, while showing no noteworthy deactivation over the experimental time.

In the experiments with C28, less fuel was supplied to the FR compared to ilmenite and braunite. Due to the lower density of C28, only lower *SCR* were achieved, which made it necessary to reduce the fuel input. On the other hand, the system was sensitive that the fuel input could not be reduced much further in the experiments with the natural ores without significant temperature drops due to heat losses. Therefore, for the purpose of comparability the performace parameters combustion efficiency and carbon capture rate are plotted against the specific *SCR*, shown in Fig. 11. For a clear presentation, the operating points with ilmenite only with wood as fuel are included. The combustion efficiency shows the clear trend to higher values with increased *SCR*. The OC requires a different *SCR* for the conversion of a certain amount of fuel. C28 achieved the highest values regarding the combustion efficiency. Red marked, Ilmenite_2.1 reached the highest value of the natural ores and does not fit the trend of the rest of the ilmenite OP. The reason can be seen in the higher temperatures and an activation of the ore on the second experimental day, whereby this behavior is also known in literature [38]. With higher SCR_{spec}, the combustion efficiency was increased for each OC. This effect was limited due to the operation stability based on the the reactor design. The instabilites appeared by flooding of the countercurrent column or a temperature decrease due to heat losses. In addition, the right diagramm in Fig. 11 shows that the carbon capture rate is decreasing with higher specific *SCR*. In this diagramm, non-autothermal OP of braunite were excluded, because of the inaccuracy in determination with the addition of oil in the AR. Furthermore, braunite showed different carbon capture rates on different experimental days, probably due to the high attrition rate and the necessity to replace it with fresh material. Measured on individual days, braunite showed the same trend as the other OC, seen as dashed

Table 6
Operating points with different natural ores and C28 at 80 kWth pilot plant at TU Wien (all values calculated with a confidents interval of 95 % based on measurement accuracy and the IPSEpro simulation. The values of the most important measurements are compared with the calculated results of the IPSEpro simulation in Table 1 of the supplementary material for OP Lana_1.3.).

Operating point name	Fuel	Bed material	Fuel power input FR	Fuel power oil	Solid circulation rate	OC to fuel ratio	S/C ratio	Air to fuel ratio	Gas AR	Gas FR	Lower FR	O_2 demand	Carbon capture rate	Combustion efficiency	CO_2 yield	CO_2 selectivity
OP		OC	$P_{fuel,FR}$	P_{oil}	SCR	φ	S/C	λ	ϑAR_{exh}	ϑFR_{exh}	ϑFR_{low}	Ω_{OD}	η_{CC}	η_{comb}	γ_{CO2}	S_{CO2}
[text]	[text]	[text]	[kW]	[kW]	[kg/h]	[–]	[–]	[–]	[°C]	[°C]	[°C]	[%]	[%]	[%]	[%]	[%]
Ilmenite_1.1	Soft wood	Ilmenite	64.3	20.5	2266	5.2	1.7	1.5	910	884	865	31.3	98.7	68.7	66.8	67.7
Ilmenite_1.2	Soft wood	Ilmenite	61.3	14.6	2344	5.6	1.8	1.6	930	915	876	26.8	98.2	73.2	81.7	83.2
Ilmenite_1.3	Soft wood	Ilmenite	70.8	0.0	2434	5.1	1.3	1.4	976	975	915	17.7	98.0	82.3	86.7	88.5
Ilmenite_2.1	Soft wood	Ilmenite	74.0	0.0	1838	3.7	0.7	1.3	1018	1014	942	13.2	98.6	86.8	88.9	90.2
Braunit_1.1	Soft wood	Sibelco Braunite	54.7	21.3	1195	3.2	1.9	1.9	929	902	919	23.3	98.9	76.7	85.3	86.3
Braunit_1.2	Soft wood	Sibelco Braunite	80.5	0.0	1356	2.5	1.2	1.3	968	984	938	18.4	95.3	81.6	84.1	88.2
Braunit_1.3	Soft wood	Sibelco Braunite	77.9	0.0	972	1.9	1.2	1.4	960	981	912	23.3	95.8	76.8	81.2	84.8
Braunit_2.1	Soft wood	Sibelco Braunite	82.4	2.3	1278	2.3	1.2	1.2	965	981	939	19.4	98.8	80.6	80.6	81.6
Braunit_2.2	Soft wood	Sibelco Braunite	74.1	0.0	571	1.2	1.3	1.4	940	960	867	30.3	94.6	69.7	74.5	78.8
Braunit_2.3	Soft wood	Sibelco Braunite	80.6	0.0	885	1.7	1.2	1.3	959	972	912	19.3	93.9	80.7	81.8	87.1
Bark_1.1	Bark	Ilmenite	77.7	0.0	1726	3.2	1.1	1.3	916	920	876	18.1	94.9	81.9	82.9	87.4
Bark_1.2	Bark	Ilmenite	78.2	0.0	1734	3.2	0.8	1.2	914	913	869	17.4	95.2	82.6	85.4	89.8
Lignite_1.1	Lignite	Ilmenite	80.3	0.0	1534	3.2	1.1	1.2	930	934	889	8.0	95.4	92.0	87.6	91.9
Lignite_2.1	Lignite	Ilmenite	77.1	20.0	1799	3.4	0.8	1.2	904	906	867	11.6	98.0	88.4	89.3	91.2
Waste_2.1	Waste	Ilmenite	85.4	6.9	1165	1.9	0.7	1.1	918	887	852	20.3	97.3	79.7	55.7	57.2
ChickenManure_2.1	Chicken manure	Ilmenite	69.2	2.6	1150	2.4	0.9	1.4	918	918	860	10.7	95.6	89.3	86.8	90.7
MnOre_1	Soft wood	Mn-Ore	55.5	19.8	422	1.1	1.5	1.8	904	876	794	32.0	88.3	68.0	65.3	74.0
Lana_1.1	Bark	C28	49.9	0.0	1102	4.5	1.9	1.2	970	937	857	1.3	98.3	98.7	97.3	99.0
Lana_1.2	Bark	C28	47.7	0.0	901	2.8	2.0	1.3	978	943	847	2.3	98.1	97.7	96.2	98.1
Lana_1.3	Bark	C28	39.2	0.0	1285	7.2	2.3	1.6	949	923	867	0.8	97.6	99.2	97.2	99.6
Lana_1.4	Soft wood	C28	57.6	0.0	1385	5.8	1.7	1.0	1001	961	888	3.3	97.2	96.7	95.1	97.8
Lana_2.1	Soft wood	C28	54.1	0.0	946	4.2	1.6	1.1	1013	971	875	2.9	98.1	97.1	96.6	98.5
Lana_2.1	Soft wood	C28	52.2	0.0	1032	4.7	1.7	1.2	1011	978	889	1.9	97.9	98.1	96.9	99.0
Lana_2.1	Soft wood	C28	48.2	0.0	1164	5.8	1.8	1.2	1004	974	901	1.9	97.8	98.1	96.8	98.9

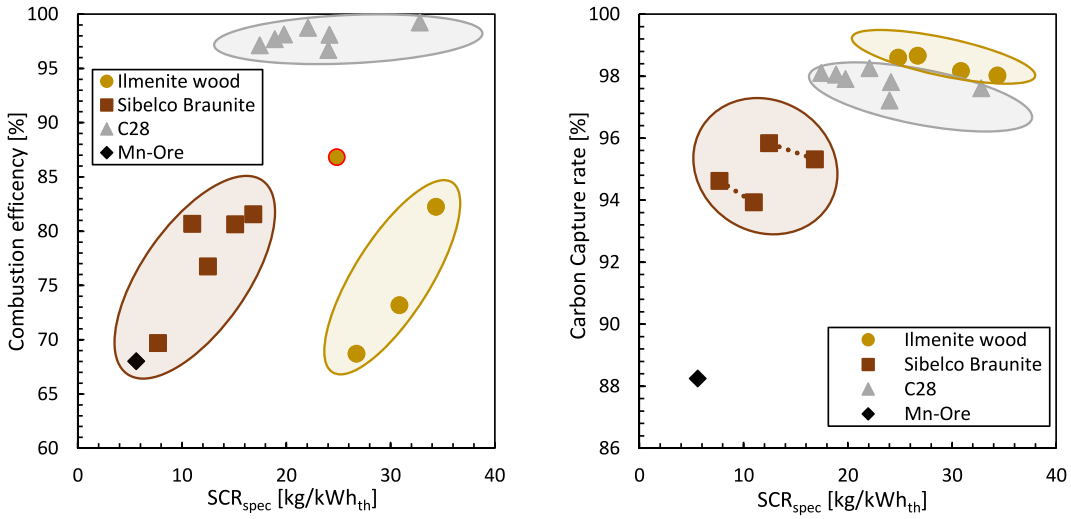

Fig. 11. Comparison of performance parameters of C28 to the natural ores, ilmenite, braunite and Mn-Ore, represented by the specific solid circulation rate.

lines in Fig. 11. With higher circulation rates and thus lower residence time, more unconverted char sliped to the AR and therefore the corresponding carbon could not be captured. Ilmenite showed the highest capture rate, even higher than the synthetic OC C28. Due to the high density of ilmenite, the bubbling bed of the lower FR is densely packed. The assumption is that the char is abraded and has therefore more pronounced contact with the OC. C28 compensated the disadvantage of lower density with its high reactivity as well as higher oxygen tranport capcity. Carbon capture rates up to 98 % were achieved with the synthetic OC C28. The fuel input and the *SCR* had an additional major impact on the temperature condtitionsin the reactors. Especially the temperature of the lower FR proved to be important for a fast gasification reaction of solid fuel and a reduction of the carbon slip to the AR. Fig. 12 shows the correlation between the specific *SCR* and the temperature of the lower fuel reactor. The temprature ϑFR_{low} is increasing with higher *SCR*. The gradient varies considerably with different fuels, based on the concentration of ash and water of the introduced fuel. The temperatures in the reactor are highly depending on the process conditions and can manually only be adapted by oil addition into the AR. The high specific heat loss via the reactor wall has a particular negative effect, because it is not possible to reach higher temperatures in the FR. In plants of larger scale, the specific temperature loss would be decreased because of the size and better insulation by refractory lining. This means that OC with good results in the 80 kW_{th} unit would probably have even more potential in larger plants with an optimized reactor design.

3.4. Counter current columns measurements

Other important design adaptations to the FR are the height and the constrictions of the counter current column. A higher FR leads to longer residence time and a more pronounced contact between gas and OC. As long as the gas conversion is limited exclusively by kinetics, the operation efficiencies could be increased by that modification of the upper FR. During a steady-state experiment with C28, converting soft wood pellets for over 5 h, the gas concentrations at different heights of the FR were measured. Fig. 13 shows the dry and nitrogen free gas concentration of CO_2, H_2, CO and CH_4 over the reactor height. The lowest measurement was carried out directly above the bubbling bed of the lower FR. Additional bypass measurements were taken below each constriction of the counter current column. The concentration of CO_2 could be increased from 75 % at the bubbling bed to over 98 % at the end of column. Most of the remaining unburnt components react in the area of the first constriction to CO_2. The measurement showed that methane was the

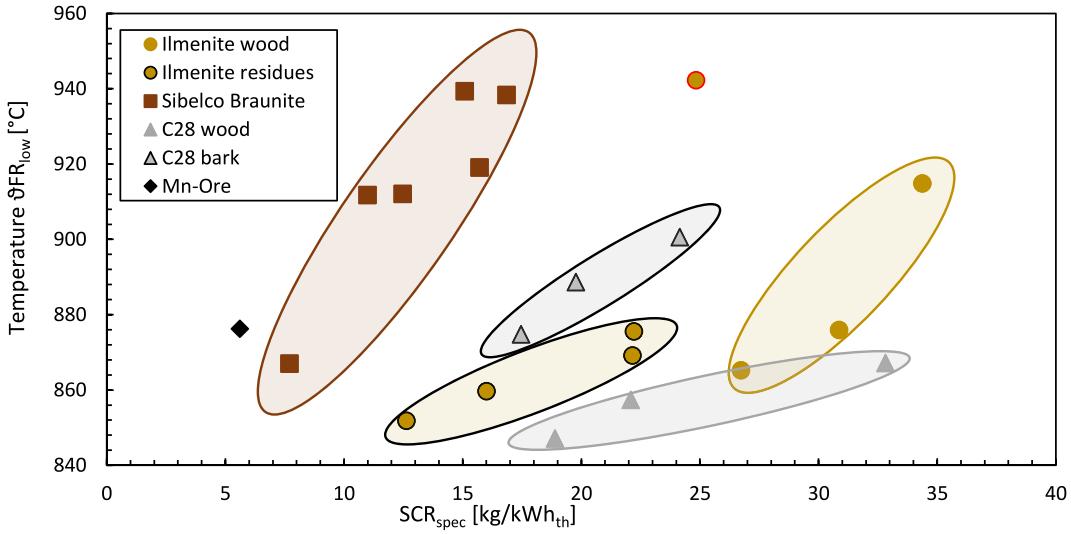

Fig. 12. Temperature dependency of the lower FR with regard to the specific solid circulation rate, C28 in comparison to natural ores with different fuels.

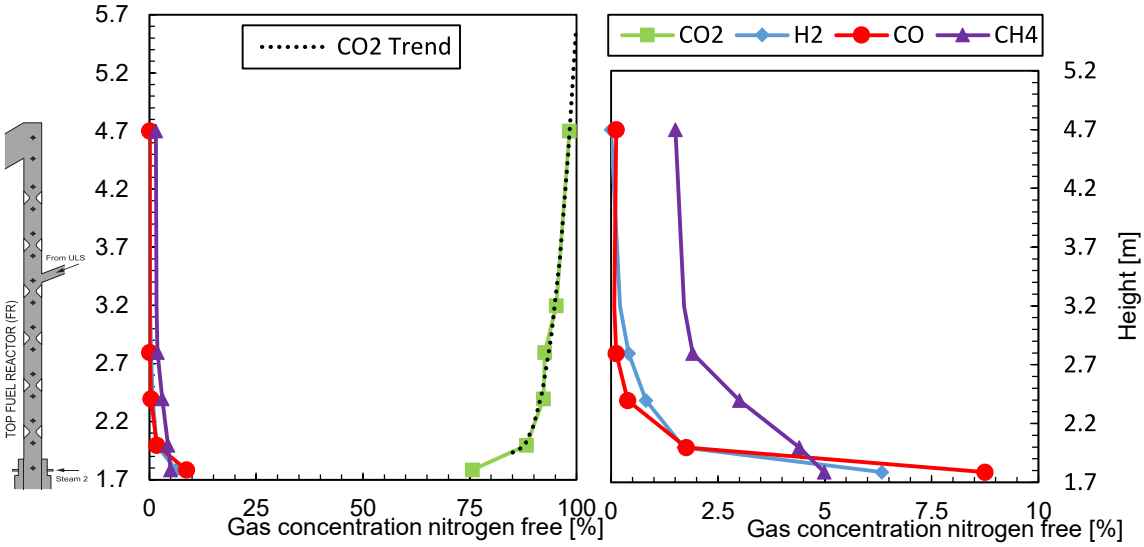

Fig. 13. Gas concentrations in the counter current column of the FR with C28 as OC and soft wood as fuel.

most stable component. The hydrogen concentration decreased slowly, due to the decomposition of methane producing new hydrogen. The measurement of CO was below the detection range of the used measurements device and was also measured with a device in ppm accuracy. The CO concentration was reduced to around 1200 ppm over the column. The operation could have been optimized by increasing the *SCR* to reach higher gas conversion. This was avoided targeting stable operation without any disruptions, like the risk of flooding the column or discharging OC. For the experiment, the CO_2 concentration with a height extension could be estimated by a polynomial approach based on the measurements. With a column height increase of 0.5 m, the CO_2 concentration could exceed 99.5 %. The increase of the height would have a proportional higher effect with higher solid circulation rates and the experimental data in this case was collected with moderate circulation rate. The increase in reactor height should be placed below the bed material entrance at the ULS, which is located at 3.5 m in the current FR setup. This would result in extended gas solid contact with hot oxidized OC. However, the increase of FR height will only benefit the conversion, as long as the chemical equilibrium is not reached and the kinetics are still fast enough to convert the low concentrations of unburnt gas.

In the further course of the experiments, the constrictions of the FR were adapted to improve gas/solid contact and gas conversion. In addition to the existing constrictions, which reduce the free cross section to 35.6 %, a tube can be inserted at each constriction to further reduce the area of the counter current column to 20.3 % of the total free cross section, see Fig. 5. This can be realized by moving the brown rod [39]. The constrictions were narrowed until just before limiting occurred due to flooding of the reactor. 1 cm of inserting the rod equals a decrease of

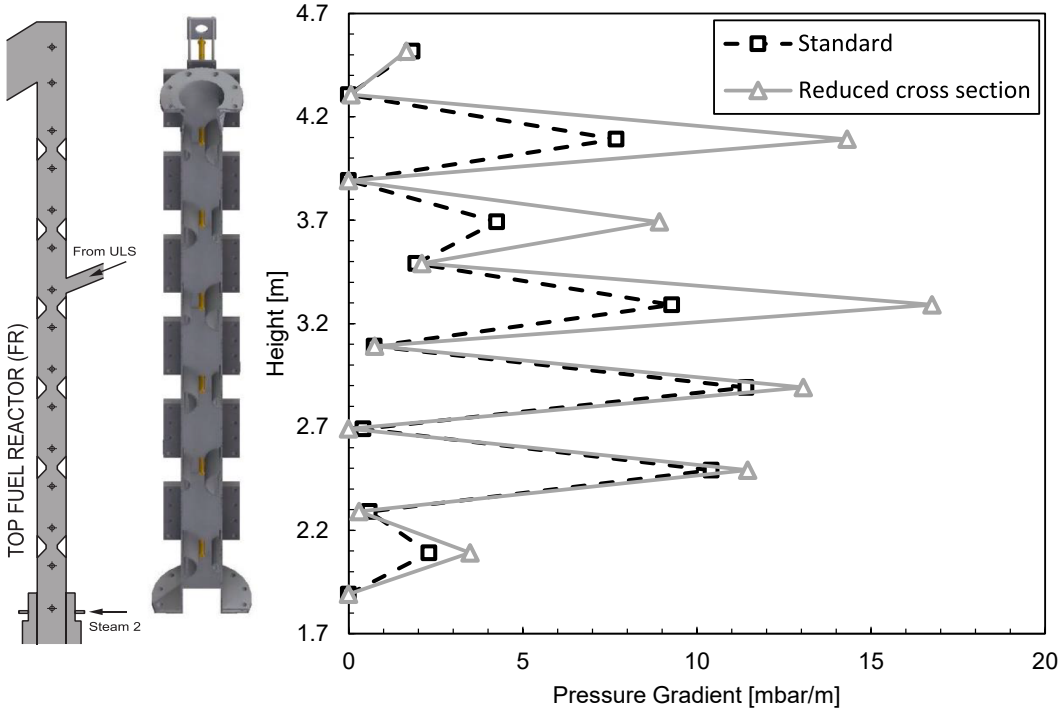

Fig. 14. Comparison of pressure gradient in the counter current column FR, standard constrictions to reduces cross section by pipe insertion.

1.2 % of the total cross section of the FR. While the rod of the fifth and sixth constriction were inserted to the half of the reactor, about 6 cm, the other constrictions from first to fourth were only inserted 2 cm. Due to the change in transverse sections, increased accumulation of bed material took place above the reduced cross section of the constrictions, see Fig. 14. The pressure gradient indicates the amount of bed material, which was located at this area of the FR during the experiment. This led to an increased mass of OC accumulating in the constricted areas and therefore to a more pronounced gas solid contact. The gas concentration can be influenced to higher conversion rates due to these interactions. During the experiments, the CO_2 concentration could be increased by 0.4 % to 93.1 %, while the CO concentration decreased by 150 ppm (both, not nitrogen corrected). A change of the methane concentration was outside the detection range of the measurement device. When comparing the effects of the constrictions to an increase of the *SCR*, both proved to be beneficial for gas conversion by increasing the hold up of bed material in the counter current column. However, the impact of the *SCR* is more severe due to an additional increase of oxygen and heat transport. Expansion of the constrictions and higher circulation rates, both are limited by flooding of the counter current column by backlog of bed material. For this reason, if the operation is close to flooding, it is more efficient to increase the *SCR* than the severity of the constrictions. However, when *SCR* is limited due to other factors or the carbon capture rate should not be decreased, the expansion of the constrictions is a viable way of improving the gas conversion. This is true for the present pilot plant, since constrictions are already inherently installed. Consequently, a statement about operation without constrictions cannot be made for this setup. On industiral scale, the installation of constriction would lead to a higher fan power and addition costs. Cosnstrictions would nevertheless pay off,s if the cost of gas cleaning steps like oxy-polsihing could be ommitted or be reduced this way.

3.5. Alteration of C28

In order to investigate structural and compositional changes of the synthetic bed material, further analysis of solid samples from the experiment in 80 kW_{th} pilot plant were performed and compared to fresh material. Fig. 15 shows cross sections of fresh (a) and used (b) bed material, obtained via scanning electron microscope. Comparing the two samples, a structural change in the particle after the experiment in 80 kW_{th} pilot plant could be observed. A smooth, non-porous layer surrounds the particle and underneath, a porous region could be identified (Fig. 15c and d). Energy-dispersive X-ray spectroscopy analysis also discovers a slight accumulation of K, Al and Si – the most abundant components in fuel ash – in the layer. Howbeit, the majority of the layer has the same composition as the fresh bed material, which indicates the alternation of phase structure, rather than the enrichment of particular elements.

Table 7 provides results of XRD analyses of both fresh and used bed particles. In fresh particles, calcium manganite perovskite with the formula $CaTi_{0.1}Mn_{0.9}O_{2.96}$ is the most dominant phase. Small amounts of calcium titanium oxide and periclase could be also identified. Interestingly, 7.6 % of fresh material consists of $CaMn_2O4$. $CaMn_2O_4$ is a non-perovskite phase which is formed at high temperature in reducing conditions [40] and hinders the complete regeneration of perovskite during consecutive redox cycles. Consequently, a decrease in CLOU properties of oxygen carrier could be observed [41]. Uncoupling of oxygen from perovskite corresponds to the following reaction [27]:

$$CaMn_{0.775}Mg_{0.1}Ti_{0.125}O_{2.9} \rightarrow CaMn_{0.9}Mg_{0.1}Ti_{0.125} + 0.075O_2$$

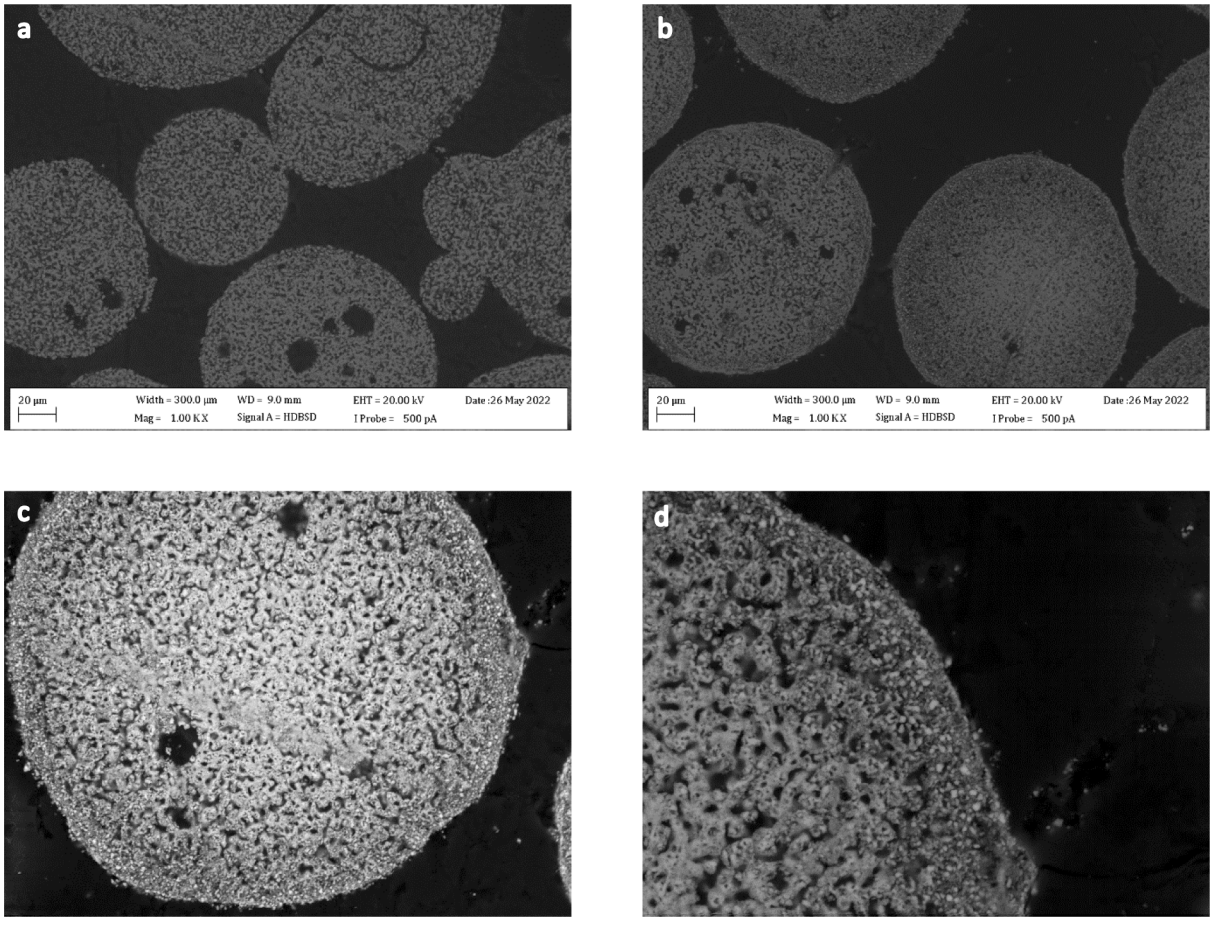

Fig. 15. Backscattered electron micrograph of (a and c) fresh bed material, (b and d) used bed material.

Table 7
Main phases in fresh and used bed material, identified by XRD analysis.

Phase	Chemical formula	Fresh material	Used material
Calcium manganese titanium oxide	$CaTi_{0.1}Mn_{0.9}O_{2.96}$	83.6	8.2
Calcium titanium oxide	$CaTiO_3$	3.9	4.6
Marokite	$CaMn_2O_4$	7.6	36.5
Periclase	MgO	4.9	5.3
Armacolite	$MgTi_2O_5$	–	10.4
Calcium manganese oxide	$CaMnO_3$	–	13.7
Calcium titanium oxide	$Ca_{0.1}TiO_2$	–	1.4
Calcium manganese oxide	$CaMnO_{2.99}$	–	12.4
Donwilhelmsite	$CaAl_4Si_2O_{11}$	–	7.6

Such release of gaseous oxygen is possible only while the perovskite structure is maintained. Formation of non-perovskite phases such as $CaMn_2O_4$ or Ca_2MnO_4 at the expense of original perovskite material is therefore highly undesirable. Though, examining the used particles, a clear shift towards non-perovskite structure after the experiments could be observed. The major part of original calcium manganite perovskite has decomposed, forming additional $CaMn_2O_4$ as well as calcium manganese and titanium oxides. The newly formed stochiometric and unstochiometric phases are presumably responsible for structural changes near the particle surface. Fig. 16 depicts surface morphology of fresh and used particles. The fresh, unused particles are covered with irregularities, such as spherical excesses. The used particles on the other hand show a much smoother, spherical surface with a less porous structure, but deposits of fines on the surface. However, according to BET analysis, the surface area of the particles almost tripled in comparison to fresh material (Table 8). However, it is hardly possible to distinguish between the formation of porous structures or the deposition of fine particles.

All in all, no pronounced deactivation or ash layers on the surface could be detected over the experimental duration. However, the beginnings of ash deposition, dilution with ash, phase shifting and fine particle formations could be seen. These can lead to considerable degradation of operation for long-term experiments and are especially critical for expensive synthetic oxygen carriers. During the experiments, an increase in the surface area was even observed, hence maintained reactivity and high conversion rates.

4. Conclusion

In this work synthetic C28 was investigated for its suitability as oxygen carrier in an 80 kW_{th} pilot plant for chemical looping combustion with solid fuels. The influence of operating parameters such as the solid circulation rate or the free area of constrictions was examined. A comparison was drawn with former experimental campaigns with different natural ores. In addition, the role of the countercurrent column of the fuel reactor was studied with C28 and its deactivation over the duration of the experiment was analyzed. The findings can be summarized as follows:

- C28 proved to be a highly viable oxygen carrier, reaching CO_2 selectivity's up to 99.6 % and high carbon capture rates up to 98,3 %.
- The solid circulation rate, a most essential parameter, favored the temperature in the fuel reactor and the gas conversion, but had negative effects on the carbon capture rate.
- In contrast to natural ores, C28 showed higher reactivity especially to the components CH_4, CO and H_2 with a lower total filling of bed material in the reactor.
- The synthetic oxygen carrier C28 suffered no deactivation nor degradation over the experimental time, but first traces of ash layer formation, phase shifting and attrition of fines could be detected. This are critical factors for high price synthetic oxygen carriers.
- The counter current column played a major role in th conversion of unburnt gases. The constricted areas have to be ideally balanced to the solid circulation rate in order to avoid flooding and still achieving the highest possible gas–solid contact and consequently highest conversion rates.

The focus of further research should lie on investigating long-term stability and reactivity for their high impact on the economic scale up of chemical looping combustion with C28. The role of the fuel ash will be an important factor, because the separation of C28 from ash seems not feasible. Furthermore, it must be verified whether the low concentration of unburnt gases mainly CO for storage application can actually be achieved without an oxy-polishing step. Unless these requirements are fulfilled, it is unlikely that C28 will be economical suitable for chemical looping combustion of solid fuels in a larger scale. This also shows that synthetic oxygen carriers need further improvement and research.

Table 8
Surface are measured with BET of fresh and used bed material.

	Unit	Fresh	Used
Surface area	m^2/g	0.5188	1.4489

Declaration of Competing Interest

The authors declare that they have no known competing financial interests or personal relationships that could have appeared to influence the work reported in this paper.

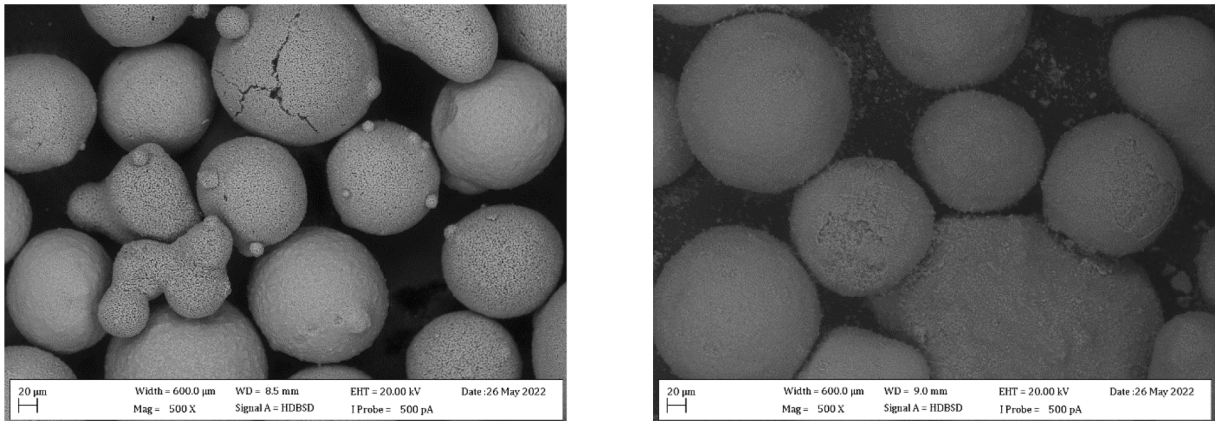

Fig. 16. Backscattered electron micrograph of bed particle surface of fresh material (left) and used bed material (right).

Data availability

Data will be made available on request.

Acknowledgements

The present work is part of the Research Project BIO-LOOP of the cooperation partners BEST – Bioenergy and Sustainable Technologies GmbH (BEST), TU Graz: Institute of Chemical Engineering and Environmental Technology (CEET) and Institute for Thermal Engineering (ITE); National Institute of Chemistry: Department of Materials Chemistry; Spanish National Research Council: Department of Energy and Environment; Chalmers University of Technology; Rouge H2 Engineering GmbH; AVL List GmbH; Aichernig Engineering GmbH; Christof Project GmbH; SW-Energie Technik GmbH; TG Mess-, Steuer- und Geotechnic GmbH; Rohkraft – Ing. Karl Pfiehl GmbH. The COMET Module BIO-LOOP (Austrian Research Promotion Agency Project Number 872189) is funded within COMET – Competence Centers for Excellent Technologies – by the Federal Ministry for Climate Action, Environment, Energy, Mobility, Innovation and Technology (BMK), the Federal Ministry for Digital and Economic Affairs (BMDW) as well as the co-financing federal province Styria (SFG). The COMET programme is managed by FFG (Austrian Research Promotion Agency, the funding is gratefully acknowledged. The authors also acknowledge TU Wien Bibliothek for financial support through its Open Access Funding Programme.

Appendix A. Supplementary data

Supplementary data to this article can be found online at https://doi.org/10.1016/j.fuel.2022.126816.

References

[1] Adánez J, Abad A, Mendiara T, Gayán P, de Diego LF, García-Labiano F. Chemical looping combustion of solid fuels. Prog Energy Combust Sci 2018;65:6–66.
[2] S. Solomon, D. Qin, M. Manning, Z. Chen, M. Marquis, K.B. Averyt, M. Tignor, H.L. Miller, (2007), Climate Change 2007: The Physical Science Basis. Contribution of Working Group I to the Fourth Assessment Report of the Intergovernmental Panel on Climate Change, IPCC, 4.
[3] Rydén M, Lyngfelt A, Langørgen Ø, Larring Y, Brink A, Teir S, et al. Negative CO_2 Emissions with Chemical-Looping Combustion of Biomass – A Nordic Energy Research Flagship Project. Energy Procedia 2017;114:6074–82.
[4] Lyngfelt A, Brink A, Langørgen Ø, Mattisson T, Rydén M, Linderholm C. 11,000 h of chemical-looping combustion operation—Where are we and where do we want to go? Int J Greenhouse Gas Control 2019;88:38–56.
[5] Pachler RF, Penthor S, Mayer K, Hofbauer H. Fate of sulfur in chemical looping combustion of gaseous fuels using a Perovskite oxygen carrier. Fuel 2019;241:432–41.
[6] Pachler RF, Penthor S, Mayer K, Hofbauer H. Investigation of the fate of nitrogen in chemical looping combustion of gaseous fuels using two different oxygen carriers. Energy 2020;195.
[7] Adánez J, Abad A. Chemical-looping combustion: Status and research needs. Proc Combust Inst 2019;37:4303–17.
[8] T. Pröll, 2011, Innovative fuel conversion with CO2 capture using dual fluidized bed systems, in: Habilitation treatis, TU Wien, Vienna, pp. 200.
[9] I. Adánez-Rubio, H. Bautista, M.T. Izquierdo, P. Gayán, A. Abad, J. Adánez, (2021), Development of a magnetic Cu-based oxygen carrier for the chemical looping with oxygen uncoupling (CLOU) process, Fuel Processing Technology, 218.
[10] Abad A, Adánez-Rubio I, Gayán P, García-Labiano F, de Diego LF, Adánez J. Demonstration of chemical-looping with oxygen uncoupling (CLOU) process in a 1.5kWth continuously operating unit using a Cu-based oxygen-carrier. Int J Greenhouse Gas Control 2012;6:189–200.
[11] T. Pröll, H. Hofbauer, (2010), A dual fluidized bed system for chemical looping combustion of solid fuels, Proceedings of the AIChE Annual Meeting 2010 Salt Lake City, USA.
[12] J. Schmid, T. Pröll, C. Pfeifer, H. Hofbauer, 2011, Improvement of gas-solid interaction in dual circulating fluidized bed systems, in: Proceedings of the 9th Conference on Industrial Furnances and Boilers (INFUB-9) Estoril, Portugal.
[13] Penthor S, Stollhof M, Pröll T, Hofbauer H. Detailed fluid dynamic investigations of a novel fuel reactor concept for chemical looping combustion of solid fuels. Powder Technol 2016;287:61–9.
[14] Pröll T, Kolbitsch P, Bolhàr-Nordenkampf J, Hofbauer H. A novel dual circulating fluidized bed system for chemical looping processes. AIChE J 2009;55:3255–66.
[15] Schmid JC, Müller S, Hofbauer H. First scientific results with the novel dual fluidized bed gasification test facility at TU Wien. In: 24th European Biomass Conference and Exhibition (EUBCE). Amsterdam, The Netherlands: ETA-Florence Renewable Energies; 2016. p. 842–6.
[16] Benedikt F, Fuchs J, Schmid JC, Müller S, Hofbauer H. Advanced dual fluidized bed steam gasification of wood and lignite with calcite as bed material. Korean J Chem Eng 2017;34:2548–58.
[17] Fuchs J, Schmid J, Müller S, Hofbauer H. Sorption Enhanced Reforming: Transport Characteristics of CO_2 and Char. in: 11th International Conference on Sustainable Energy & Environmental Protection. Paisley, United Kingdom: University of the West of Scotland; 2018.
[18] Mauerhofer AM, Benedikt F, Schmid JC, Fuchs J, Müller S, Hofbauer H. Influence of different bed material mixtures on dual fluidized bed steam gasification. Energy 2018;157:957–68.
[19] Müller S, Fuchs J, Schmid JC, Benedikt F, Hofbauer H. Experimental development of sorption enhanced reforming by the use of an advanced gasification test plant. Int J Hydrogen Energy 2017;42:29694–707.
[20] Penthor S, Fuchs J, Benedikt F, Schmid J, Mauerhofer A, Mayer K, et al. First results from an 80 kW dual fluidized bed pilot unit for solid fuels at TU Wien. in: 5th International Conference on Chemical Looping. Utah, USA: Park City; 2018.
[21] Mattisson T, Adánez J, Mayer K, Snijkers F, Williams G, Wesker E, et al. Innovative Oxygen Carriers Uplifting Chemical-looping Combustion. Enrgy Proced 2014;63:113–30.
[22] Penthor S, Mattisson T, Adánez J, Bertolin S, Masi E, Larring Y, et al. The EU-FP7 Project SUCCESS – Scale-up of Oxygen Carrier for Chemical Looping Combustion using Environmentally Sustainable Materials. Enrgy Proced 2017;114:395–406.
[23] Moldenhauer P, Hallberg P, Biermann M, Snijkers F, Albertsen K, Mattisson T, et al. Oxygen-Carrier Development of Calcium Manganite-Based Materials with Perovskite Structure for Chemical-Looping Combustion of Methane. Energ Technol 2020;8.
[24] Jacobs M, van der Kolk T, Albertsen K, Mattisson T, Lyngfelt A, Snijkers F. Synthesis and upscaling of perovskite Mn-based oxygen carrier by industrial spray drying route. Int J Greenhouse Gas Control 2018;70:68–75.
[25] Mayer K, Piesenberger S, Penthor S, Pröll T, Hofbauer H. Chemical Looping Combustion Using Two Different Perovskite Based Oxygen Carriers: A Pilot Study. Energy Technology; 2018.
[26] Cuadrat A, Abad A, Adánez J, de Diego LF, García-Labiano F, Gayán P. Behavior of ilmenite as oxygen carrier in chemical-looping combustion. Fuel Process Technol 2012;94:101–12.
[27] Abad A, García-Labiano F, Gayán P, de Diego LF, Adánez J. Redox kinetics of $CaMg_{0.1}Ti_{0.125}Mn_{0.775}O_{2.9-\delta}$ for Chemical Looping Combustion (CLC) and Chemical Looping with Oxygen Uncoupling (CLOU). Chem Eng J 2015;269:67–81.
[28] Fleiß B, Penthor S, Müller S, Hofbauer H, Fuchs J. Holistic assessment of oxygen carriers for chemical looping combustion based on laboratory experiments and validation in 80 kW pilot plant. Fuel Processing Technology; 2022. p. 231.
[29] Marx K, Bertsch O, Pröll T, Hofbauer H. Next Scale Chemical Looping Combustion: process Integration and Part Load Investigations for a 10MW Demonstration Unit. Energy Procedia 2013;37:635–44.
[30] Bolhàr-Nordenkampf J, Pröll T, Kolbitsch P, Hofbauer H. Comprehensive Modeling Tool for Chemical Looping Based Processes. Chem Eng Technol 2009;32:410–7.
[31] Wagner W, Kruse A. Properties of water and steam: The industrial standard IAPWS-IF97 for the thermodynamic properties and supplementary equations for other properties : tables based on these equations. Berlin: Springer; 1998.
[32] Burcat A, Gardiner WC. Ideal Gas Thermochemical Data for Combustion and Air Pollution. New York: Springer; 2000.
[33] Barin I, Platzki G. Thermochemical Data of Pure Substances. Wiley-VCH Verlag GmbH; 1995.
[34] Adanez J, Abad A, Garcia-Labiano F, Gayan P, de Diego LF. Progress in Chemical-Looping Combustion and Reforming technologies. Prog Energy Combust Sci 2012;38:215–82.
[35] Kolbitsch P, Pröll T, Bolhar-Nordenkampf J, Hofbauer H. Characterization of Chemical Looping Pilot Plant Performance via Experimental Determination of Solids Conversion. Energy Fuel 2009;23:1450–5.
[36] Fuchs J, Schmid JC, Benedikt F, Mauerhofer A, Müller S, Hofbauer H. A general method for the determination of the entrainment in fluidized beds, The. Int J Multiphys 2018;12.
[37] von Berg L, Pongratz G, Pilatov A, Almuina-Villar H, Hochenauer C, Scharler R, et al. Correlations between tar content and permanent gases as well as reactor temperature in a lab-scale fluidized bed biomass gasifier applying different feedstock and operating conditions. Fuel 2021;305.
[38] Adánez J, Cuadrat A, Abad A, Gayán P, de Diego LF, García-Labiano F. Ilmenite Activation during Consecutive Redox Cycles in Chemical-Looping Combustion. Energy Fuel 2010;24:1402–13.
[39] R. Diem. 2015, Design, Construction and Startup of an Advanced 100 kW Dual Fluidized Bed System for Thermal Gasification, in: Institute of Chemical, Environmental and Bioscience Engineering, TU Vienna, Vienna.
[40] Bakken E, Norby T, Stolen S. Nonstoichiometry and reductive decomposition of CaMnO. Solid State Ion 2005;176:217–23.
[41] Rydén M, Lyngfelt A, Mattisson T. $CaMn_{0.875}Ti_{0.125}O_3$ as oxygen carrier for chemical-looping combustion with oxygen uncoupling (CLOU)—Experiments in a continuously operating fluidized-bed reactor system. Int J Greenhouse Gas Control 2011;5:356–66.